Edinburgh Research Explorer

Multiscale Fluctuation-based Dispersion Entropy and its Applications to Neurological Diseases

Multiscale Fluctuation-based Dispersion Entropy and its Applications to Neurological Diseases

HAMED AZAMI[1,*], **STEVEN E. ARNOLD**[1], **SAEID SANEI**[2], **(Senior Member, IEEE),**
ZHUOQING CHANG[3], **GUILLERMO SAPIRO**[4], **(Fellow, IEEE), JAVIER ESCUDERO**[5],
(Member, IEEE), and ANOOPUM S. GUPTA[6]

[1]Department of Neurology and Massachusetts General Hospital, Harvard Medical School, Charlestown, MA 02129, USA.
[2]School of Science and Technology, Nottingham Trent University, Nottingham, UK.
[3]Department of Electrical and Computer Engineering, Duke University, Durham, NC 27707, USA.
[4]Department of Electrical and Computer Engineering, Computer Sciences, Biomedical Engineering, and Math, Duke University, Durham, NC 27707, USA.
[5]School of Engineering, Institute for Digital Communications, University of Edinburgh, Edinburgh, UK.
[6]Department of Neurology and Massachusetts General Hospital, Harvard Medical School, Boston, MA 02114, USA.

Corresponding author: Hamed Azami (e-mail: hazami@mgh.harvard.edu).

ABSTRACT Fluctuation-based dispersion entropy (FDispEn) is a new approach to estimate the dynamical variability of the fluctuations of signals. It is based on Shannon entropy and fluctuation-based dispersion patterns. To quantify the physiological dynamics over multiple time scales, multiscale FDispEn (MFDE) is developed in this article. MFDE is robust to the presence of baseline wanders or trends in the data. We evaluate MFDE, compared with popular multiscale sample entropy (MSE), multiscale fuzzy entropy (MFE), and the recently introduced multiscale dispersion entropy (MDE), on selected synthetic data and five neurological diseases' datasets: 1) focal and non-focal electroencephalograms (EEGs); 2) walking stride interval signals for young, elderly, and Parkinson's subjects; 3) stride interval fluctuations for Huntington's disease and amyotrophic lateral sclerosis; 4) EEGs for controls and Alzheimer's disease patients; and 5) eye movement data for Parkinson's disease and ataxia. MFDE avoids the problem of undefined MSE values and, compared with MFE and MSE, leads to more stable entropy values over the scale factors for white and pink noises. Overall, MFDE is the fastest and most consistent method for the discrimination of different states of neurological data, especially where the mean value of a time series considerably changes along the signal (e.g., eye movement data). This study shows that MFDE is a relevant new metric to gain further insights into the dynamics of neurological diseases recordings.

INDEX TERMS Complexity, multiscale fluctuation-based dispersion entropy, biomedical signals, electroencephalogram, stride interval fluctuations, eye movements.

I. INTRODUCTION

One of the most popular and powerful nonlinear measures used to evaluate the dynamical characteristics of signals is entropy [1]–[4]. Shannon entropy (ShEn) and conditional entropy (ConEn) are two key fundamental concepts in information theory widely used for characterization of physiological signals [2], [3]. ShEn and ConEn show the amount of information and rate of information production, respectively, and are related to the uncertainty or irregularity of data [2]–[5]. A higher entropy value demonstrates higher irregularity, while smaller entropy values show lower irregularity or uncertainty in a time series [2], [4], [6].

Existing entropy techniques, such as sample entropy (SampEn), fuzzy entropy (FuzEn), and permutation entropy (PerEn), are widely used to quantify the irregularity of signals at one temporal scale [4], [5], [7]. However, these techniques fail to account for the multiple time scales inherent in biomedical recordings [8], [9]. To deal with this limitation, multiscale SampEn (MSE) was proposed [10] and it has become a prevalent algorithm to quantify the complexity of univariate time series, especially physiological recordings [8], [11].

Following [8], [10], the concept of complexity stands for "meaningful structural richness", which may be in contrast

with uncertainty or irregularity of time series defined by classical entropy approaches such as SampEn and PerEn [4], [8], [12], [13]. As mentioned above, these entropy approaches evaluate repetitive patterns and return maximum values for completely random processes [8], [13], [14]. However, a completely ordered time series with a low entropy value or a completely disordered signal with a high entropy value is the least complex [8], [13], [15]. For instance, white noise is more irregular than pink noise ($1/f$ noise) even though the latter is more complex since the pink noise has long-range correlations and its $1/f$ decay produces a fractal structure in time [8], [13], [15].

In brief, the concept of complexity builds on three hypotheses: I) the complexity of a physiological time series indicates its ability to adapt and function in an ever-changing environment; II) a biological time series requires to operate across multiple temporal scales and so, its complexity is similarly multiscaled and hierarchical; and III) a wide class of disease states, in addition to aging, decrease the adaptive capacity of the individual, thus reducing the information carried by output variables. Therefore, the MSE focuses on quantifying the information expressed by the physiologic dynamics over multiple temporal scales [8], [13].

In spite of its popularity, MSE is undefined or unreliable for very short signals and computationally expensive for real-time applications as a result of using SampEn [9], [16]. To address the first shortcoming, refined composite MSE (RCMSE) [17], multiscale FuzEn (MFE) [18], and refined composite MFE (RCMFE) [9], [19], [20] have been developed. However, RCMSE, MFE, and RCMFE are even slower for some real-time applications. Furthermore, RCMSE may still lead to undefined or unreliable results for short signals [9].

To address the high computational time of MSE, MFE, RMCSE and RCMFE, multiscale PerEn (MPE) has been proposed [16]. Although MPE is considerably faster than MSE and MFE, it does not fulfill the key hypotheses of the concept of complexity as described above [21]. For example, white noise would be considered more complex than white noise using MPE, which is in contradiction with the results obtained by MSE and MFE [9]. Furthermore, the behaviour of MPE is different from that of MSE in some cases so, in reality, MPE does not replace MSE in all aspects [9], [21]. To overcome the limitations of MPE, MFE, and MSE, RCMFE, and RCMSE at the same time, we have recently introduced multiscale dispersion entropy (DispEn - MDE) and refined composite MDE (RCMDE), based on our developed DispEn [4], [22], to quantify the complexity of signals [23].

Compared with the conventional complexity approaches, 1) MDE and RCMDE increase the reliability of the results and at the same time do not lead to undefined values for short signals, 2) MDE and RCMDE are markedly faster, especially for long signals, and 3) they yield larger differences between physiological conditions, such as subjects with epilepsy disorders or Alzheimer's disease (AD) vs. matched controls [23].

The complexity methods have been applied in different research fields, including biomedical engineering and neuroscience [11], [24]. MSE was successfully used for the diagnosis of depression using heart rate variability, speech recordings, and electroencephalograms (EEGs) [25]. Using MSE, an increased EEG signal complexity was found in Parkinson's disease (PD) patients during non-rapid eye movement sleep at high scale factors [26]. MDE was successfully used for sleep stage classification using single-channel electrooculography signals [27]. Miskovic *et al.* showed that slow sleep EEG data were characterized by reduced MDE values at low scales and increased MDE values at high scale factors [28]. MDE, MFE, and MSE were used to discriminate AD patients from age-matched controls using magnetoencephalogram signals [9], [29]. The differences between the MDE values for the AD vs. healthy subjects were more significant than their corresponding MSE-based values.

In many real-world applications (e.g., in computing the correlation function and in spectral analysis), the (local or global) trends from a signal [30], [31] need to be removed. In such methods, after detrending the local or global trends of a time series, the fluctuations are evaluated [30], [31]. When only the fluctuations of data are relevant or local trends of a time series are irrelevant [30]–[32], there is no difference between dispersion patterns $\{11\}$, $\{22\}$, and $\{33\}$ or $\{12\}$ and $\{23\}$. That is, the fluctuations of $\{11\}$, $\{22\}$, and $\{33\}$ or $\{12\}$ and $\{23\}$ are equal as we are interested in the relative rather than absolute values. Thus, we have very recently introduced fluctuation-based DispEn (FDispEn) [22]. The potential of FDispEn for characterization of various synthetic and biomedical data was shown. For example, FDispEn significantly discriminated eleven 3-4 years old children from twelve 11-14 years old subjects using their stride interval fluctuations [22]. However, this was never extended to multiscale for covering a wider range of applications.

Therefore, the main contributions of this study are proposing multiscale FDispEn (MFDE) and refined composite MFDE (RCMFDE) and evaluating these techniques on selected synthetic signals and five neurological datasets: focal and non-focal EEGs, stride interval fluctuations in PD, young and elderly individuals as well as Huntington's disease (HD) and amyotrophic lateral sclerosis (ALS), resting-state EEG activity in AD, and eye movement data in ataxia vs. PD.

This article is structured as follows. In Section II, the MFDE and RCMFDE algorithms are detailed. The synthetic and real datasets used here are briefly described in Section III. The results and discussion are provided in Section IV. After describing future works in Section V, we conclude the paper in Section VI.

II. METHODS

A. MULTISCALE FLUCTUATION-BASED DISPERSION ENTROPY (MFDE)

MFDE is based on the coarse-graining process [8] and FDispEn [22]. Assume we have a univariate signal of length L:

$u = \{u_1, u_2, ..., u_L\}$. In the MFDE algorithm, the original signal **u** is first divided into non-overlapping segments of length τ, named scale factor. Afterwards, the average of each segment is calculated to derive a coarse-grained time series as follows [8]:

$$x_j^{(\tau)} = \frac{1}{\tau} \sum_{b=(j-1)\tau+1}^{j\tau} u_b, \quad 1 \leq j \leq \left\lfloor \frac{L}{\tau} \right\rfloor = N \quad (1)$$

Of note is that other coarse-graining processes can be used in this step [24], but, for the sake of clarity, we focus on the original definition in this paper. Finally, the FDispEn of each coarse-grained signal $x_j^{(\tau)}$ is calculated.

The FDispEn of the univariate signal of length N: $x = \{x_1, x_2, ..., x_N\}$ is defined as follows:

Step 1) First, $x_j (j = 1, 2, ..., N)$ are mapped to c classes with integer indices from 1 to c. To this end, the normal cumulative distribution function (NCDF) is first utilized to overcome the problem of assigning the majority of x_i to only few classes, especially when thr maximum or minimum values are noticeable larger or smaller than the mean/median value of the signal [4], [22], [23]. For more information about the reasons behind using NCDF, please see [4], [22].

The NCDF maps x into $y = \{y_1, y_2, ..., y_N\}$ from 0 to 1 as follows:

$$y_j = \frac{1}{\sigma\sqrt{2\pi}} \int_{-\infty}^{x_j} e^{\frac{-(t-\mu)^2}{2\sigma^2}} \, \mathrm{d}t, \quad (2)$$

where σ and μ are the standard deviation (SD) and mean of time series **x**, respectively. Then, we linearly assign each y_i to an integer from 1 to c. To do so, for each member of the mapped signal, we use $z_j^c = \text{round}(c \cdot y_j + 0.5)$, where z_j^c denotes the jth member of the classified time series and the rounding operator involves either increasing or decreasing a number to the next digit [4], [22], [23].

Step 2) Time series $z_i^{m,c}$ are defined with respect to embedding dimension $m-1$ and time delay d according to $z_i^{m,c} = \{z_i^c, z_{i+d}^c, ..., z_{i+(m-1)d}^c\}, i = 1, 2, ..., N - (m-1)d$ [4], [22]. Each time series $z_i^{m,c}$ is mapped to a fluctuation-based dispersion pattern $\pi_{v_0 v_1 ... v_{m-1}}$, where $z_i^c = v_0$, $z_{i+d}^c = v_1,..., z_{i+(m-1)d}^c = v_{m-1}$. The number of possible fluctuation-based dispersion patterns that can be assigned to each time series $z_i^{m,c}$ is equal to $(2c-1)^{(m-1)}$ [22].

Step 3) For each $(2c-1)^{m-1}$ potential dispersion patterns $\pi_{v_0...v_{m-1}}$, relative frequency is obtained as follows:

$$p(\pi_{v_0...v_{m-1}}) = \frac{\#\{i \,|\, i \leq N - (m-1)d, \mathbf{z}_i^{m,c} \text{ has type } \pi_{v_0...v_{m-1}}\}}{N - (m-1)d}, \quad (3)$$

where $\#$ means cardinality. In fact, $p(\pi_{v_0...v_{m-1}})$ shows the number of dispersion patterns of $\pi_{v_0...v_{m-1}}$ that is assigned to $z_i^{m,c}$, divided by the total number of embedded signals with embedding dimension m.

Step 4) Finally, based on Shannon's definition of entropy, the FDispEn value is calculated as follows:

$$FDispEn(\mathbf{x}, m, c, d) = \\ - \sum_{\pi=1}^{(2c-1)^{m-1}} p(\pi_{v_0...v_{m-1}}) \cdot \ln\left(p(\pi_{v_0...v_{m-1}})\right), \quad (4)$$

It is worth noting that the mapping based on the NCDF used in the calculation of FDispEn [4] for the first temporal scale is maintained across all scales. In fact, in MFDE, μ and σ of NCDF are respectively set at the average and SD of the original signal and they remain constant for all scale factors. This approach is similar to keeping r constant (usually 0.15 of the SD of the original signal) in the MSE-based algorithms [8].

FDispEn deals with the differences between adjacent elements of dispersion patterns, named fluctuation-based dispersion patterns [22]. In this way, we have vectors with length $m-1$, which each of their elements changes from $-c + 1$ to $c-1$. Thus, there are $(2c-1)^{m-1}$ potential fluctuation-based dispersion patterns. For instance, let us have a series $x = \{3.6, 4.2, 1.2, 3.1, 4.2, 2.1, 3.3, 4.6, 6.8, 8.4\}$, shown on the top left of Fig. 1. We want to calculate the FDispEn value of **x**. For simplicity, we set $d = 1$, $m = 2$, and $c = 3$. The five potential fluctuation-based dispersion patterns vs. nine potential dispersion patterns are depicted on the right of Fig. 1. Step 1: $x_j (j = 1, 2, ..., 10)$ are linearly mapped into three classes with integer indices from 1 to 3, as can be seen in Fig. 1. Step 2: a window with length 2 (embedding dimension) moves along the signal and the number of each of the fluctuation-based dispersion patterns is counted. Step 3: the relative frequency for both DispEn and FDispEn are shown on the bottom left of Fig. 1. Step 4: using Equation (4), the FDispEn value of **x** is equal to $-(\frac{4}{9}\ln(\frac{4}{9}) + \frac{3}{9}\ln(\frac{3}{9}) + \frac{2}{9}\ln(\frac{2}{9})) = 1.0609$.

When all possible fluctuation-based dispersion patterns have equal probability value, the highest value of FDispEn is obtained, which has a value of $ln((2c-1)^{m-1})$. In contrast, if there is only one $p(\pi_{v_0...v_{m-1}})$ different from zero, which demonstrates a completely regular/predictable time series, the smallest value of FDispEn is obtained [22].

B. REFINED COMPOSITE MULTISCALE FLUCTUATION-BASED DISPERSION ENTROPY (RCMFDE)

For completeness, we also describe RCMFDE. This is based on the idea of considering τ versions of the coarse-grained sequence at each temporal scale. Each version of the coarse-grained sequence corresponds to a different starting point of the coarse-graining process. Then, for each of these shifted series, the relative frequency of each fluctuation-based dispersion pattern is calculated. Finally, the RCMFDE value is defined as the Shannon entropy value of the averages of the rates of appearance of fluctuation-based dispersion patterns of those shifted sequences [23], [24].
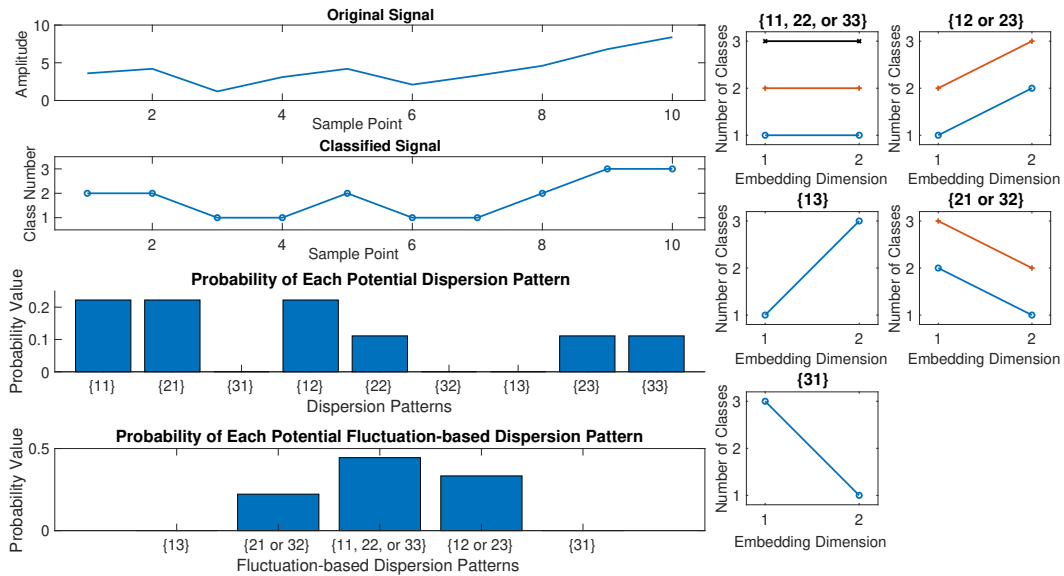
FIGURE 1: Illustration of the FDispEn vs. DispEn algorithms using linear mapping of $x = \{3.6, 4.2, 1.2, 3.1, 4.2, 2.1, 3.3, 4.6, 6.8, 8.4\}$ (top left) with the time delay 1, number of classes 3, and embedding dimension 2. The nine dispersion patterns $\{11, 12, 13, 21, 22, 23, 31, 32, 33\}$ and five fluctuation-based dispersion patterns $\{11, 12, 13, 21, 31\}$ are shown on the right of Figure. The relative frequency for both DispEn and FDispEn are illustrated on the bottom left of Figure.

III. EVALUATION SIGNALS

To assess the ability of MFDE, compare it with MFE, MSE, and MDE, and to characterize various univariate time series, we use the following synthetic and neurological datasets.

A. SYNTHETIC SIGNALS

1) The complexity of pink noise ($1/f$ noise) is higher than white noise, whereas the irregularity or uncertainty of the former signal is lower than the latter [8], [13], [23]. Thus, white and pink noise are two suitable data for assessing the multiscale entropy techniques [8], [13], [15], [21], [33]. For more information about white vs. pink noise, please refer to [8], [34].

2) Physiological signals are often corrupted by different kinds of noise, such as additive white Gaussian noise (WGN) [35]. A WGN is also considered as a basic statistical model used in information theory to mimic the effect of random processes that occur in nature [36]. In order to understand the relationship between MFDE, MSE, and MDE, and the level of noise affecting periodic time series, we generated an amplitude-modulated periodic signal with a WGN with diverse power. First, we generated a time series as an amplitude-modulated sum of two cosine waves with frequencies at 0.5 Hz and 1 Hz. The first 20 s of this series (100 s) does not have any noise. Then, WGN was added to the time series [34].

B. NEUROLOGICAL DATASETS

Diagnosing of people with neurological diseases from healthy subjects, or among different neurological diseases, by analysis of their recorded time series is a long-standing challenge in the physiological complexity literature [8], [23],

[26], [37]–[39]. EEGs, walking stride interval time series, and eye movement are clinical pavements that may be helpful in diagnosis and tracking of neurological diseases states [6], [23], [39], [40]. Using these recordings, MFDE, MDE, and MSE are used to characterize several neurological diseases such as ALS, AD, PD, cerebellar ataxias, and HD.

1) Dataset of Focal and Non-focal Electroencephalograms (EEGs): Epilepsy is a common neurological condition. EEG signals are used to identify areas that generate or propagate by seizures [39], [41]. Generally, focal EEG signals are recorded from the epileptic part of the brain, whereas non-focal EEGs correspond to brain regions unaffected by epilepsy [41]. The ability of MFDE, MDE, and MSE to discriminate focal from non-focal signals is evaluated by the use of an EEG dataset (publicly-available at [42]) [39].

The dataset includes 5 patients and, for each patient, there are 750 focal and 750 non-focal bivariate time series. The length of each signal was 20 s with sampling frequency of 512 Hz (10240 samples). Focal and non-focal EEG time series samples are depicted in Fig. 2. For more information, please, refer to [39]. All subjects gave written informed consent that their signals from long-term EEG might be used for research purposes [39]. Before applying the complexity methods, the time series were digitally filtered using a Hamming window FIR band-pass filter of order 200 and cut-off frequencies 0.5 Hz and 40 Hz, a band typically used in the analysis of brain activity.

2) Dataset of Walking Stride Interval Time Series for Young, Elderly, and Parkinson's Disease (PD) Subjects: It was shown that aging leads to less complex recordings of stride [8], [40]. It was also documented that the gait of ALS
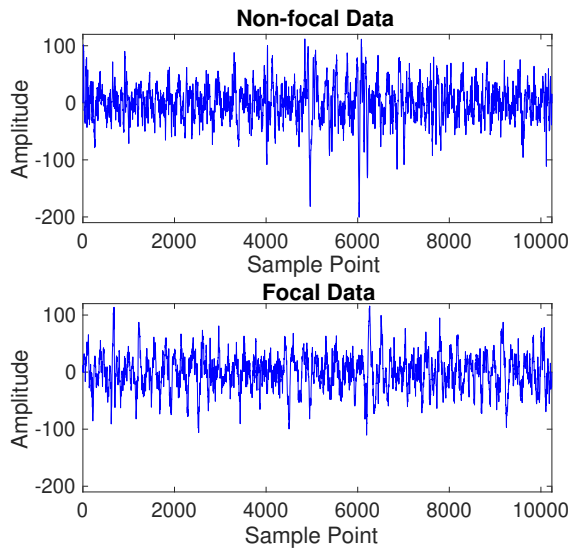
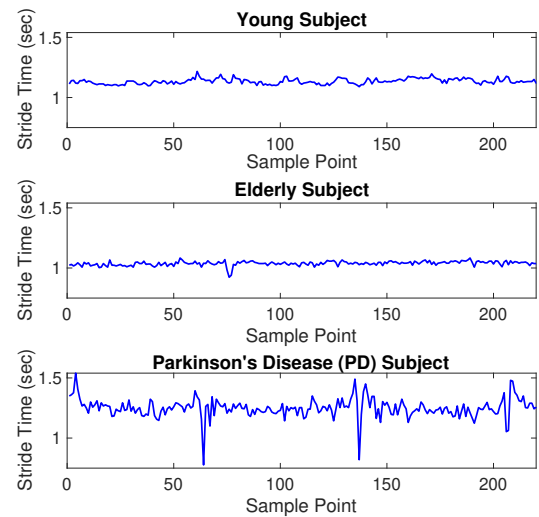FIGURE 2: Example of a focal and non-focal EEG time series.

FIGURE 3: Example of effects of aging and Parkinson's disease on fluctuations of stride-interval dynamics.

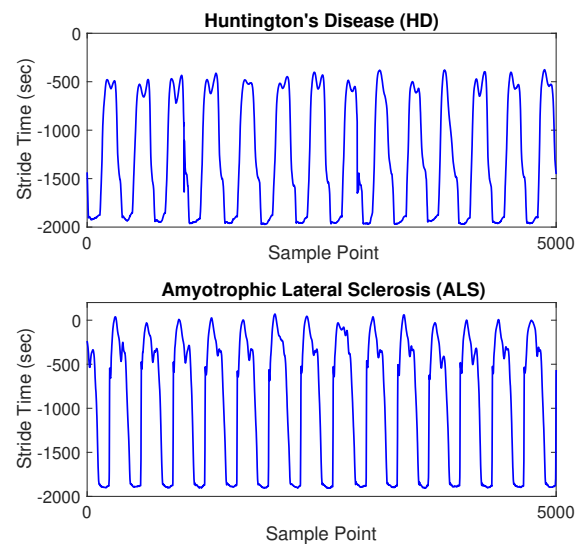

FIGURE 4: Example of effects of amyotrophic lateral sclerosis and Huntington's disease on fluctuations of stride-interval dynamics.

patients is less stable and more temporally disorganized in comparison with that of healthy individuals. Furthermore, advanced ALS, HD, and PD were associated with certain common, but also distinct, features of altered stride dynamics [40], [43]. To this end, we use the walking stride interval fluctuations to distinguish PD patients from healthy elderly subjects, young from elderly people, and ALS from HD patients (next dataset).

To compare MFDE, MDE, MFE, and MSE, publicly-available stride interval recordings were used [40], [44]. The signals were recorded from five young, healthy men (23 - 29 years old), five healthy old adults (71 - 77 years old), and five elderly adults (60 - 77 years old) with PD. All the individuals walked continuously on level ground around an obstacle-free path for 15 minutes. The stride interval was measured by the use of ultra-thin, force sensitive resistors placed inside the shoe. Fig. 3 shows an example of the stride-interval time series for a young, an elderly, and a PD subject. For more information, please refer to [44].

3) Dataset of Walking Stride Interval Time Series for Huntington's Disease (HD) vs. Amyotrophic Lateral Sclerosis (ALS) Patients: For the HD subjects, there is an increased randomness in stride interval fluctuations as compared with healthy people [40], [43]. On the other hand, gait usually becomes abnormal during the course of the ALS disease. A decreased (average) walking velocity was reported in ALS [45]. It is yet unknown if the loss of motoneurons also changes the stride-to-stride complexity of gait.

The recordings, which are available at [46], are from 20 HD and 13 ALS patients. The mean age of the HD and ALS patients respectively were 47 (range 29-71) and 54.9 years (range 36-70). Subjects with ALS were able to walk independently for five minutes and did not use a wheelchair or assistive device for mobility. The subjects were instructed to walk at their normal pace along a 77-m-long hallway for

5 minutes. To measure the gait rhythm and the timing of the gait cycle, force-sensitive insoles were placed in the patients' shoes. The sampling frequency of the data was 300 Hz. Fig. 4 shows an example of the stride-interval time series for a HD and an ALS subject. Note that all the patients provided informed, written consent and the study was approved by the Massachusetts General Hospital (MGH) Institutional Review Board. For more information about the dataset, please refer to [43].

4) Surface Electroencephalogram (EEG) Dataset of Brain Activity in Alzheimer's Disease (AD): AD, as a neurodegenerative disease, is the most common form of dementia [47], [48]. AD changes the interaction between neurons in
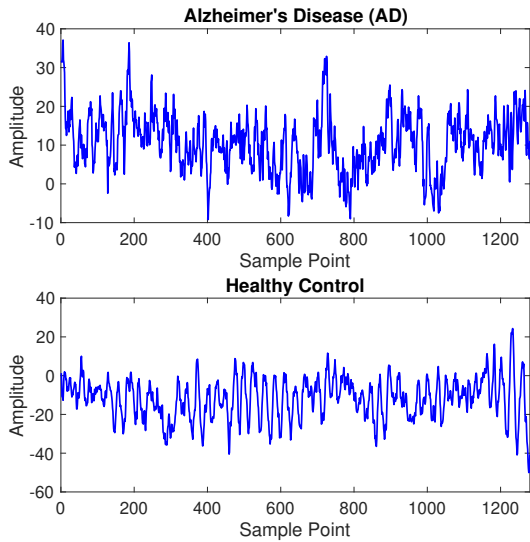
FIGURE 5: Example of effects of Alzheimer's disease on EEG time series.

FIGURE 6: Example of eye movements for Parkinson's disease vs. ataxia.

the brain during its progression. Consequently, it alters brain activity. Some of these changes may be recorded by the EEG technique [49]–[52].

The 16-channel EEG dataset includes 11 AD patients (5 men; 6 women; age: 72.5 ± 8.3 years, all data given as mean ± SD) and 11 age-matched control healthy subjects (7 men; 4 women; age: 72.8 ± 6.1 years) [53]. To screen their cognitive status, a mini-mental state examination (MMSE) [54] was done. The MMSE scores for AD patients and healthy subjects are 13.3 ± 5.6 and 30 ± 0, respectively.

The subjects were recruited from the Alzheimer's Patients' Relatives Association of Valladolid (AFAVA), Spain. The EEG time series were recorded with Oxford Instruments Profile Study Room 2.3.411 EEG equipment at the Hospital Clínico Universitario de Valladolid (Spain). The EEGs were recorded using the international 10-20 system, in an eyes closed and resting state. All 16 electrodes were referenced to the linked ear lobes of each individual. The signals were sampled at 256Hz and digitized with a 12-bit analog-to-digital converter. Informed consent was obtained for all 22 subjects and the local ethics committee approved the study. Before band-pass filtering with cut-off frequencies 1 and 40 Hz and a Hamming window with order 200, the signals were visually examined by an expert physician to select 5 s epochs (1280 samples) with minimal artifacts for analysis. On average, 30.0 ± 12.5 epochs (mean±SD) were selected from each electrode and each subject. An example of an AD EEG signal vs. an age-matched healthy control's EEG is shown in Fig. 5.

5) Eye Movement Dataset for Parkinsonism and Ataxia Patients: Neurodegenerative diseases affect oculomotor function in a variety of ways, which impact vision and also provide clues into the underlying pathology and diagnosis. Cerebellar ataxias are an heterogeneous group of inherited and acquired diseases. As a broad group, ataxias cause pro-
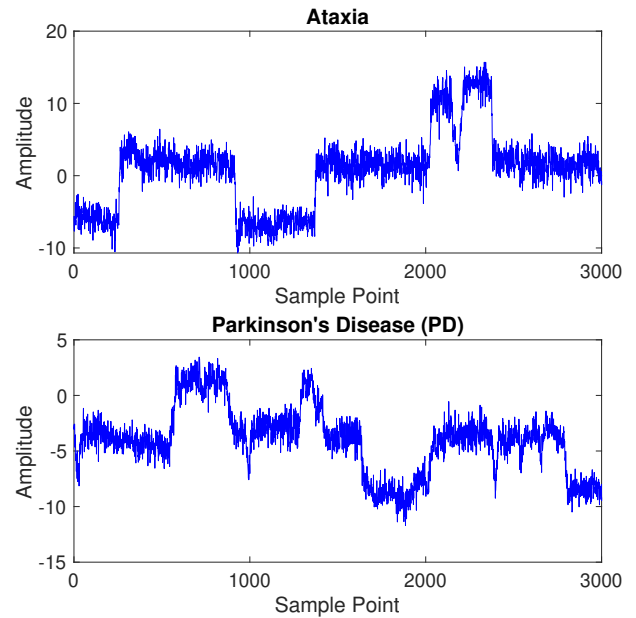
found and characteristic abnormalities in smooth pursuit, saccades, and fixation [55]. Oculomotor abnormalities in PD are clinically more subtle, but quantitative testing demonstrates abnormalities in both saccades and in smooth pursuit [56], [57].

Participants with cerebellar ataxia and parkinsonism were recruited to participate in eye movement testing in MGH Neurology clinics. Stimuli for the antisaccades task were presented on an Apple iPad screen, while simultaneously recording each participant's face from an Apple iPhone camera sampling at 240fps. The video was processed using [58] to extract facial landmarks, in particular the iris center. 57 participants with cerebellar ataxia and 20 participants with parkinsonism (18 with Parkinson's disease and 2 with atypical parkinsonism) were included in this dataset. An example of eye movements for Parkinson's disease vs. ataxia is depicted in Fig. 6.

IV. RESULTS AND DISCUSSION
A. SYNTHETIC SIGNALS
1) White and Pink Noise
Fig. 7 and Fig. 8 demonstrate the results obtained for MFDE, MDE, MSE, MFE, RCMFDE, RCMDE, RCMSE, and RCMFE using 40 different white and pink noise signals with lengths 400 and 2,000 sample points, respectively. The Refined Composite methods (RC-) are included for completeness. All the results are in agreement with the fact that pink noise has more complex structure than white noise, and white noise is more irregular than pink noise [8], [13], [15]. Thus, at short scale factors, the entropy values of white noise are higher than those of pink noise. At high scale factors the entropy value for the coarse-grained pink noise time series

stays almost constant, whereas for the coarse-grained white noise data monotonically decreases. A slightly decreasing trend in MDE for pink noise is observed, but not so much in MFDE, showing an advantage of MFDE over MDE. For white noise, when the length of the signal, obtained by the coarse-graining process, decreases (i.e., the scale factor increases), the mean value of each segment converges to a constant value and the SD at that scale becomes smaller. Therefore, no new structures are revealed on higher scales. This demonstrates white noise signals contain information only at short time scales [8], [15]. For all the methods, we set $m = 2$ and $d = 1$, according to Subsection IV.2.

For the noise signals with length 400, the MSE and RCMSE values at some high scale factors are undefined, showing that RCMSE may not be able to address the problem of undefined entropy values at high scale factors [9].

To compare the results obtained by the complexity approaches, we used the coefficient of variation (CV) at temporal scale factor 10, as a trade-off between short and long scales. CV is defined as the SD divided by the mean. We use such a metric as the SDs of signals may increase or decrease proportionally to the mean. The results, demonstrated in Table 1, show that the refined composite algorithm makes all the MSE, MDE, MFE, and MFDE more stable. MFDE- and MDE-based CV values are considerably smaller than those based on MSE or MFE. Additionally, RCMFDE and RCMDE led to the most stable results (lowest CV values) for white and pink noises, respectively.

Of note, we used the refined composite-based complexity methods for the neurological datasets. These complexity techniques considerably increased the computational time (data not shown). However, they did not improve the stability of results noticeably for the neurologic datasets, in agreement with [24], [59]. Therefore, the refined composite-based results are not shown for the following datasets.

The MFDE, MFE, MDE, and MSE methods are applied to the quasi-periodic signals with additive noise using a moving window of 450 samples (3 s) with 50% overlap. Fig. 9 demonstrates the MFDE-, MDE-, MFE-, and MSE-based profiles using the quasi-periodic signal with increasing additive noise power. As expected, the entropy values for all the four methods increase along the signal. At high scale factors, the entropy values decrease due to the filtering nature of the coarse-graining process [24]. To sum up, the results show that all the methods lead to the similar findings, although the MFE, MDE, and MFDE values are slightly more stable than the MSE ones, as demonstrated by the smoother nature of variations for MFE, MDE, and MFDE, compared with MSE. Therefore, when a high level of noise is present, MFE, MDE, and MFDE result in more stable profiles than MSE.

2) Parameters of MFDE

There are four parameters for MFDE, namely the embedding dimension m, the number of classes c, the time delay d, and the maximum scale factor τ_{max}. To work with reliable statistics to calculate FDispEn, it is recommended that the

number of potential fluctuation-based dispersion patterns is smaller than the length of the signal $((2c-1)^{m-1} < L)$ [22]. For MFDE, the coarse-graining process causes the length of a signal decreases to $\left\lfloor \frac{L}{\tau_{max}} \right\rfloor$. Therefore, it is recommended to have $(2c-1)^{m-1} < \left\lfloor \frac{L}{\tau_{max}} \right\rfloor$.

$c > 1$ must be used to avoid the trivial case of having only one fluctuation-based dispersion pattern. To assess the sensitivity of MFDE to the number of classes c, we used 40 realizations of univariate white and pink noises of 2,000 sample lengths. The mean and SD of results for $c = 3$ to 10, depicted in Fig. 10, show that pink noise is more complex than white noise for MFDE with different c values.

To compare the stability of results, we calculated CV values at scale factor 10. The results are illustrated in Table 2. $c = 7$ led to the smallest CV. Nevertheless, since we did not select the optimum parameter values for the other complexity methods and there is no noticeable difference between the CVs for $c = 6$ and $c = 7$, the number of classes is equal to 6 for both the MDE and MFDE techniques [22], [23]. Note that since the number of potential fluctuation-based dispersion patterns $(\ln((2c-1)^{m-1}))$ is higher for a higher c, the MFDE values are larger.

The mean and SD of results for $m = 2$ to 5, depicted in Fig. 11, demonstrate that MFDE is consistent with different m values. It is worth noting that because of increased computational times, we did not consider $m > 5$, although the MFDE method is still faster than the other complexity methods (please see Table 5). To compare the stability of results, we calculated CV values at scale factor 10. These are illustrated in Table 3. $m = 2$ led to the smallest CV. Therefore, for all the following experiments, we set $m = 2$ for MFDE, MFE, MDE, and MSE [8], [9], [23]. Note that for a higher m, since the number of potential fluctuation-based dispersion patterns $(\ln((2c-1)^{m-1}))$ is higher, the MFDE values are larger.

If the sampling frequency is noticeably larger than the highest frequency component of a signal, the first minimum or zero crossing of the autocorrelation function or mutual information can be used for the selection of an appropriate time delay [24], [60]. We show the results for MFDE with $d = 1$ to 8 in Fig. 12. The results do not considerably change with different time delay values. The CV values, illustrated in Table 4 at scale factor 10, show that there is no major difference between the CV values. Based on the existing complexity-based approaches [8]–[10], [16], the time delay was set to 1 for all the methods in this study.

It is worth noting that white noise is uncorrelated and its samples are independent, so, naturally, there is no difference between $d = 1$ and $d = 8$. A similar situation happens for pink noise: due to the long term correlations it has, it should be relatively independent from the choice of d. However, the time delay d may play a bigger role in band-limited signals. We will investigate the effect of d on all the complexity methods in the future.

The threshold r for MSE and MFE, which is used as a

FIGURE 7: Mean value and SD of the MFDE, MDE, MSE, MFE, RCMFDE, RCMDE, RCMSE, and RCMFE results for 40 different realizations of pink and white noise time series of 400 sample lengths. The MSE and RCMSE values are undefined at several high scale factors.
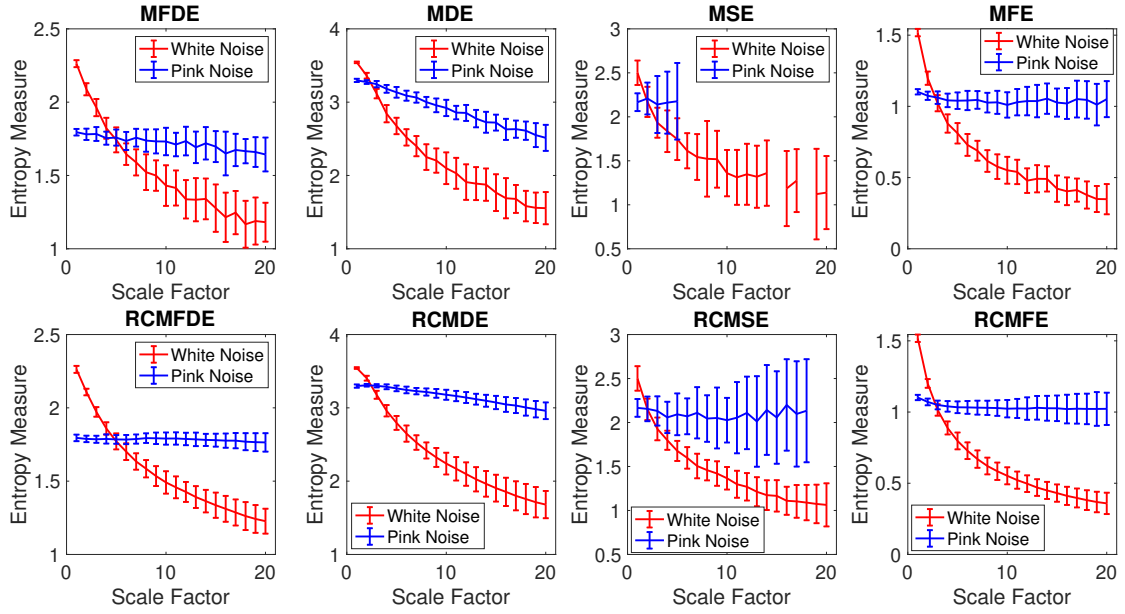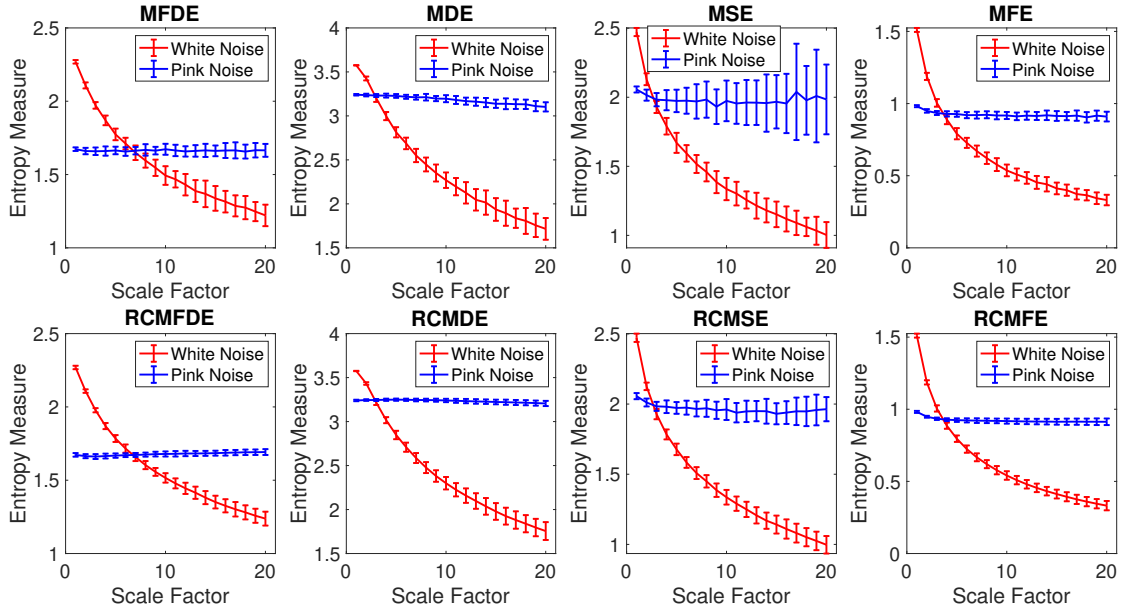

FIGURE 8: Mean value and SD of the MFDE, MDE, MSE, MFE, RCMFDE, RCMDE, RCMSE, and RCMFE results for 40 different realizations of pink and white noise time series of 2,000 sample lengths.

TABLE 1: CVs of MFDE, MDE, MSE, MFE, RCMFDE, RCMDE, RCMSE, and RCMFE at scale 10 for 40 different realizations of pink and white noises of 400 and 2,000 sample lengths.

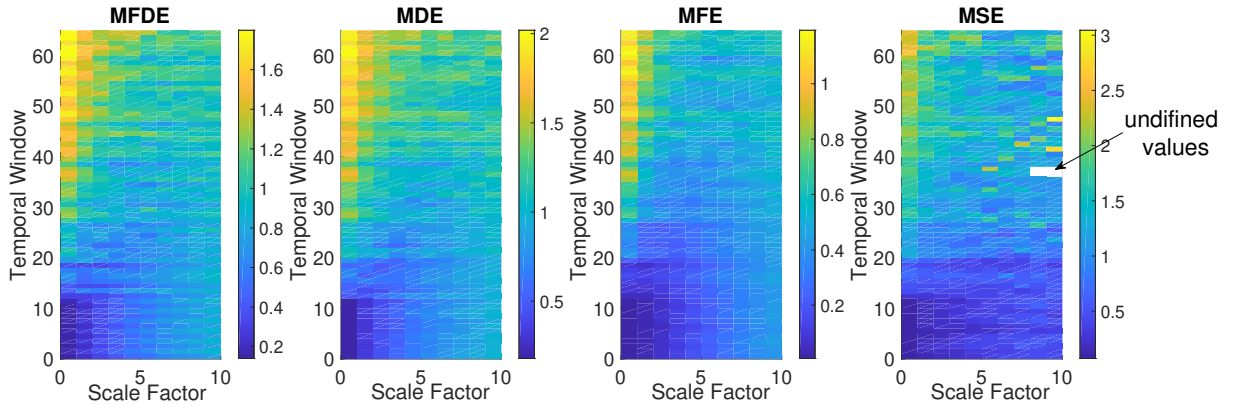| Signal	MFDE	MDE	MSE	MFE	RCMFDE	RCMDE	RCMSE	RCMFE
White noise with 400 samples	0.0979	0.1044	0.1963	0.1733	0.0518	0.0672	0.0950	0.1097
Pink noise with 400 samples	0.0548	0.0385	undefined	0.0891	0.0234	0.0217	0.1268	0.0606
White noise with 2,000 samples	0.0345	0.0348	0.0485	0.0698	0.0189	0.0240	0.0383	0.0502
Pink noise with 2,000 samples	0.0225	0.0122	0.0693	0.0303	0.0097	0.0063	0.0418	0.0217

FIGURE 9: Mean value and SD of the MFDE, MDE, MFE, and MSE results for the quasi-periodic time series with increasing additive noise power using a window moving along the signal (temporal window). The MSE values at a couple of temporal scale factors are undefined.
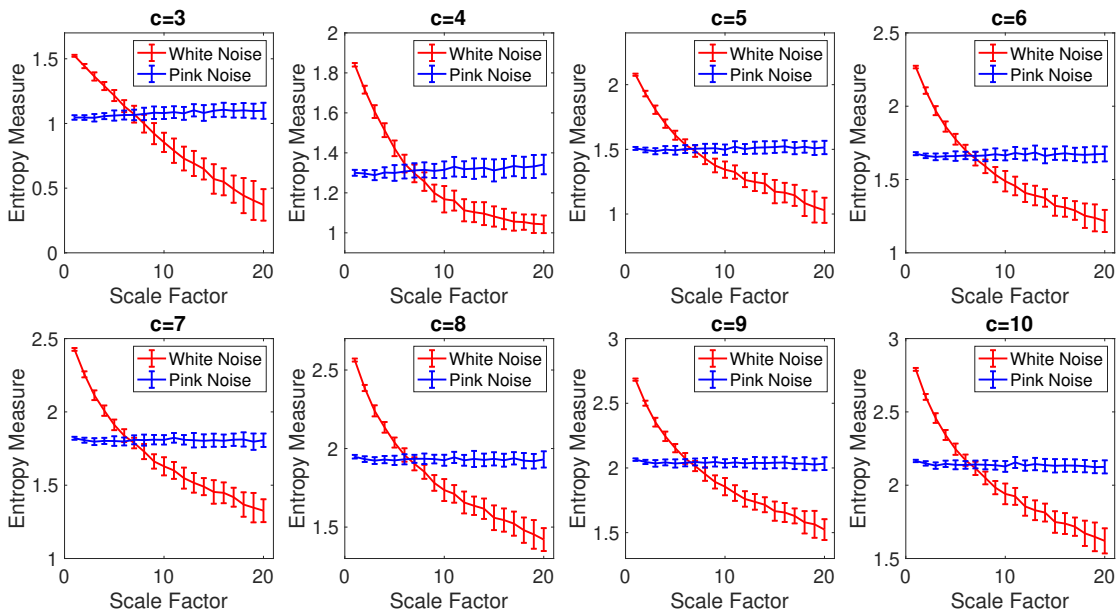

FIGURE 10: Mean value and SD of the MFDE results for different numbers of classes ($c = 3$ to 10) using 40 different realizations of pink and white noise time series of 2,000 sample lengths.

TABLE 2: CVs for MFDE with different numbers of classes ($c = 3$ to 10) at scale 10 for 40 different realizations of pink and white noises of 2,000 sample lengths.

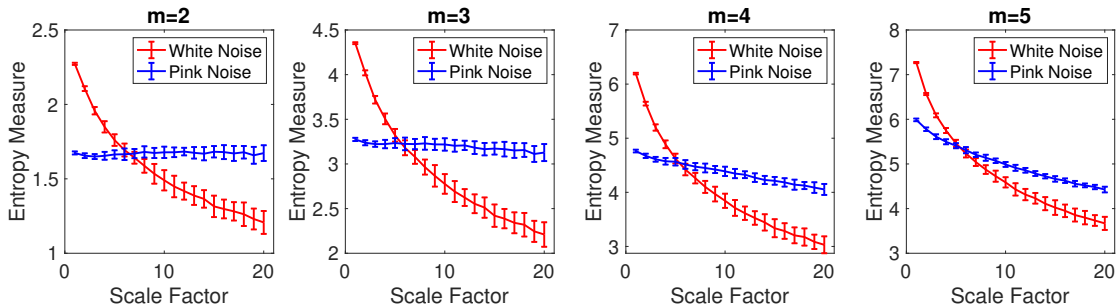| Signal	$c = 3$	$c = 4$	$c = 5$	$c = 6$	$c = 7$	$c = 8$	$c = 9$	$c = 10$
White noise	0.0403	0.0373	0.0332	0.0366	0.0320	0.0381	0.0348	0.0363
Pink noise	0.0217	0.0199	0.0195	0.0161	0.0149	0.0168	0.0151	0.0175

FIGURE 11: Mean value and SD of the MFDE results for different embedding dimension values ($m = 2$ to 5) using 40 different realizations of pink and white noise time series of 2,000 sample lengths.
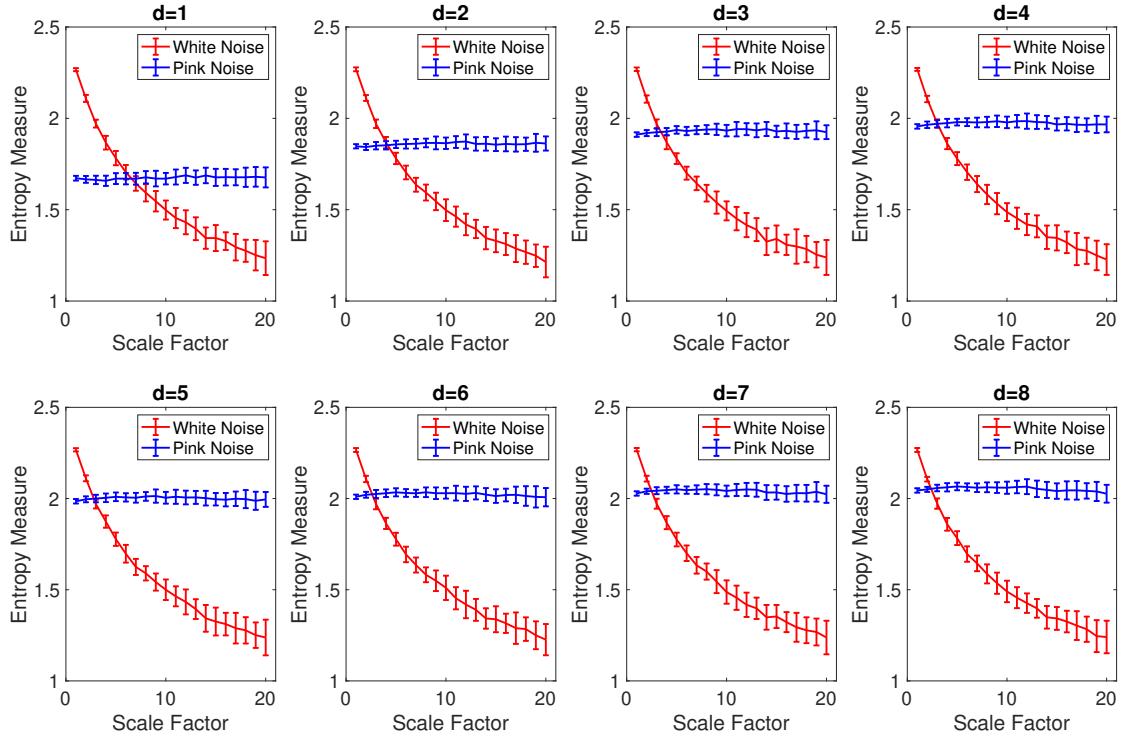
FIGURE 12: Mean value and SD of the MFDE results for different time delay values ($d = 1$ to 8) using 40 different realizations of pink and white noise time series of 2,000 sample lengths.

TABLE 3: CVs for MFDE with different embedding dimension values ($m = 2$ to 5) at scale factor 10 for 40 different realizations of pink and white noises of 2,000 sample lengths.

Signal	$m = 2$	$m = 3$	$m = 4$	$m = 5$
White noise	0.0149	0.0238	0.0281	0.0259
Pink noise	0.0077	0.0140	0.0176	0.0111

benchmark, was chosen as 0.15 of the SD of a signal [8]. Finally, for consistency, the maximum scale factor τ_{max} was set based on $c^m < \left\lfloor \frac{L}{\tau_{max}} \right\rfloor$ for all the complexity techniques used herein [23].

3) Computational Time

To evaluate the computational time of MFDE (with *m*=2 and 3 for completeness), MDE (*m*=2 and 3), MFE (*m*=2 and 3), and MSE (*m*=2 and 3), we use white noise signals with different lengths, changing from 100 to 100,000 sample points. The results are shown in Table 5. The simulations were carried out using a PC with Intel (R) Xeon (R) CPU, E5420, 2.5 GHz and 8-GB RAM by MATLAB R2015a. For 100 and 300 sample points, MSE ($m = 2$ and 3) results in undefined values at least at several scale factors. This does not happen for MDE and MFDE, demonstrating the advantage of these methods over MSE for short time series. There is no major difference between the computational time for the MSE with *m*=2 and 3. The results show that for the different numbers of sample points, MFDE and MDE are considerably faster

than MSE and MFE for long signals. This computational advantage of MFDE and MDE increases markedly with the data length. It is consistent with the fact that the computational cost of SampEn, FuzEn, FDispEn, and DispEn are $O(N^2)$, $O(N^2)$, $O(N)$, and $O(N)$, respectively [4], [21], [22]. Note that the MSE/MFE and MDE codes used in this paper are publicly-available at http://dx.doi.org/10.7488/ds/147 and http://dx.doi.org/10.7488/ds/1982, respectively.

B. NEUROLOGICAL DATASETS

In the physiological complexity literature, it is hypothesized that healthy conditions correspond to more complex states due to their ability to adapt to adverse conditions, exhibiting long range correlations, and rich variability at multiple scales, while aged and diseased individuals demonstrate complexity loss. That is, they lose the capability to adapt to such adverse conditions [8]. Therefore, we employ MFDE, compared with MDE and MSE, to characterize different pathological states using several neurological datasets. Note that we use these standard datasets only to evaluate the complexity methods, not to compete with other signal processing approaches.

1) Dataset of Focal and Non-focal EEGs: The ability of the MFDE, MDE, MFE, and MSE techniques to distinguish the focal from non-focal signals is evaluated here. The results, depicted in Fig. 13, show that the non-focal signals are more complex than the focal ones. This fact is in agreement with

TABLE 4: CVs for MFDE with different time delay values ($d = 1$ to 8) at scale factor 10 for 40 different realizations of pink and white noises of 2,000 sample lengths.

Signal	$d=1$	$d=2$	$d=3$	$d=4$	$d=5$	$d=6$	$d=7$	$d=8$
White noise with 400 samples	0.0356	0.0387	0.0360	0.0338	0.0393	0.0456	0.0452	0.0400
Pink noise with 400 samples	0.0164	0.0159	0.0163	0.0163	0.0166	0.0152	0.0150	0.0174

TABLE 5: Computational time of MFDE, MDE, MSE, and MFE for white noise with different lengths.

Number of samples $\rightarrow$	100	300	1,000	3,000	10,000	30,000	100,000
MFDE($m = 2$)	0.0028 s	0.0038 s	0.0073 s	0.0169 s	0.0463 s	0.1290 s	0.4157 s
MFDE ($m = 3$)	0.0049 s	0.0061 s	0.0097 s	0.0211 s	0.0541 s	0.1501 s	0.4945 s
MDE ($m = 2$)	0.0028 s	0.0041 s	0.0078 s	0.0176 s	0.0478 s	0.1336 s	0.4189 s
MDE ($m = 3$)	0.0053 s	0.0070 s	0.0111 s	0.0224 s	0.0598 s	0.1673 s	0.5446 s
MSE ($m = 2$)	undefined at all scales	undefined at several scales	0.0113 s	0.0743 s	0.7031 s	6.0879 s	72.1888 s
MSE ($m = 3$)	undefined at all scales	undefined at all scales	undefined at several scales	0.0681 s	0.6546 s	5.6362 s	62.3229 s
MFE ($m = 2$)	0.0066 s	0.0145 s	0.0872 s	0.5168 s	4.2218 s	30.353 s	290.091 s
MFE ($m = 3$)	0.0046 s	0.0149 s	0.0932 s	0.5781 s	4.6821 s	32.259 s	301.237 s

previous studies [39], [61]. Note that because the entropy-based methods are used for stationary signals [2], [22], we separated each signal into segments of length 2 s (1024 sample points) and applied the algorithms to each of them. The results demonstrate that all the techniques lead to the similar findings, albeit MDE and MFDE are significantly faster than MSE and MFDE ones, as illustrated in Section III. It should be mentioned that the average entropy values over 2 channels for these bivariate EEG signals are reported for these univariate complexity techniques.

The non-parametric Mann-Whitney *U*-test was employed to evaluate the differences between results for focal vs. non-focal signals at each scale factor. In this study, the scale factors with *p*-values between 0.01 and 0.05, and smaller than 0.01 are respectively shown with + and *. The *p*-values demonstrate that MFDE is the only complexity method with significant differences at all scale factors, showing its advantage over MFE, MSE, and MDE.

2) Dataset of Walking Stride Interval Time Series for Young, Elderly, and PD Subjects: As shown in Fig. 14, for most scale factors the average MFDE, MDE, MSE, and MFE values are smaller in elderly subjects compared with young subjects. This is consistent with those obtained by transfer entropy [62] and the fact that recordings from healthy young subjects correspond to more complex states due to their ability to adapt to adverse conditions, whereas older individuals' signals demonstrate complexity loss [8], [13], [63]. The results also show that the PD patients' stride interval recordings are less complex than those for the elderly subjects, which is in agreement with the fact that some diseases lead to lower complexity values [8], [10]. Since the length of each stride interval signal was between 200 to 700 samples, we did not separate the signals into smaller epochs.

The non-parametric Mann-Whitney *U*-test was employed to evaluate the differences between results for young vs. elderly individuals and elderly vs. PD patients at each scale factor. The *p*-values demonstrate that the most consistent algorithm for the discrimination of PD from elderly subjects and elderly from young individuals is MDE.

3) Dataset of Walking Stride Interval Time Series for HD vs. ALS Patients: Due to their long length, the signals were

separated into epochs of 3 s. The MFDE-, MFE-, and MSE-based results, depicted in Fig. 15, show that the stride interval fluctuations for HD are more complex than those for the ALS patients walking without any wheelchair or assistive device for mobility. This is in agreement with [40], [43]. The *p*-values show that MFE, MFDE, and MSE, unlike MDE, significantly discriminated the ALS from HD patients. Note that the only method is able to significantly discriminate the ALS from HD patients at all scale factors is MFDE.

4) Surface EEG Dataset in AD: As the length of each EEG is 5 s, we do not separate the signals into smaller epochs. MFDE, MDE, MSE, and MFE were used to characterize the time series recorded from 11 AD patients vs. 11 age-matched healthy controls. The results are depicted in Fig. 16. The average of MFDE, MDE, MFE, and MSE values for AD patients was smaller than those for healthy controls at short-time scale factors, while the AD subjects' EEGs had larger entropy values at long-time scale factors. Herein, short-time (or low) scale factors mean the temporal scales that are smaller than or equal to the scale of crossing point of the curves for AD patients vs. controls. Long-time (or high) scale factors denote the temporal scales that are larger than the scale of crossing point of the curves for AD patients vs. controls. For example, short-time and long-time scale factors are 1-12 and 13-30, respectively, for MFE in Fig. 16. All the results are consistent with [23], [37], [38], [64], [65]. Nevertheless, for MSE, unlike MDE and MFDE, values at high scale factors are undefined, showing an advantage of MFDE and MDE over MSE. Another advantage of MFDE and MDE over MSE and MFE is that these methods led to larger differences at a number of temporal scale factors. Of note is that the average of the entropy values for all the channels is reported for the univariate multiscale entropy methods herein.

5) Eye Movement Dataset for Parkinsonism vs. Ataxia Patients: To deal with the stationarity of signals, we separated each signal into epochs with length 1 s. The mean and SD of MFDE, MDE, MFE, and MSE values for parkinsonism vs. ataxia patients are depicted in Fig. 17. The results show that the mean values for all the complexity methods computed from the parkinsonism subjects are higher than those
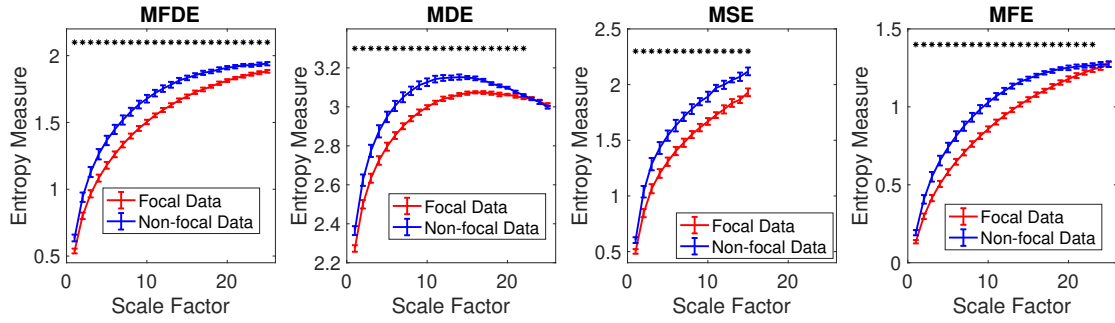
FIGURE 13: Mean value and SD of the results obtained by the MFDE, MDE, MSE, and MFE computed from the focal and non-focal EEGs. The scale factors with *p*-values between 0.01 and 0.05, and smaller than 0.01 are respectively shown with + and *. The MSE values are undefined at high scale factors.
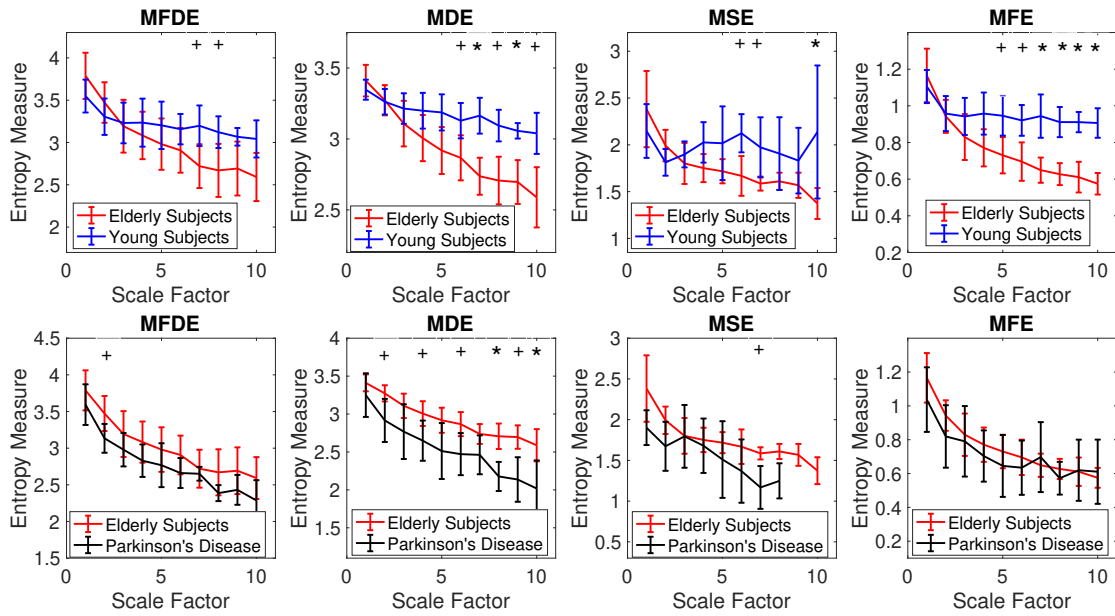

FIGURE 14: Mean value and SD of the results obtained by the MFDE, MDE, MSE, and MFE techniques computed from the young, elderly, and old Parkinson's subjects' stride interval recordings. The scale factors with *p*-values between 0.01 and 0.05, and smaller than 0.01 are respectively shown with + and *. The MSE values are undefined at high scale factors.
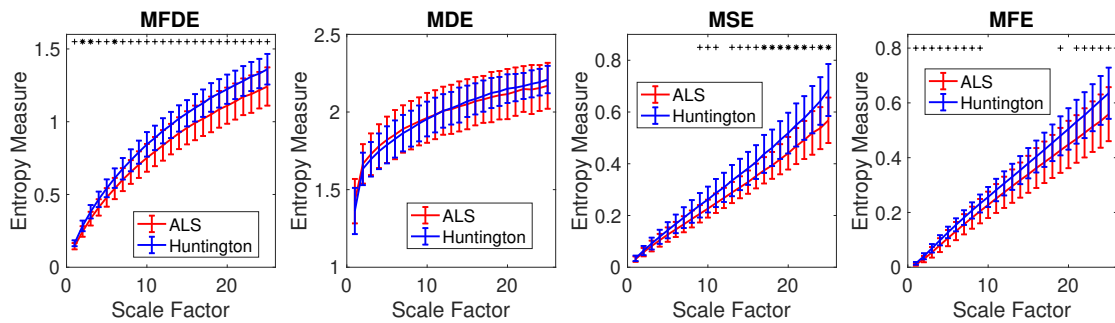

FIGURE 15: Mean value and SD of results obtained by the MFDE, MDE, MSE, and MFE techniques computed from the HD and ALS subjects' stride interval recordings. The scale factors with *p*-values between 0.01 and 0.05, and smaller than 0.01 are respectively shown with + and *.
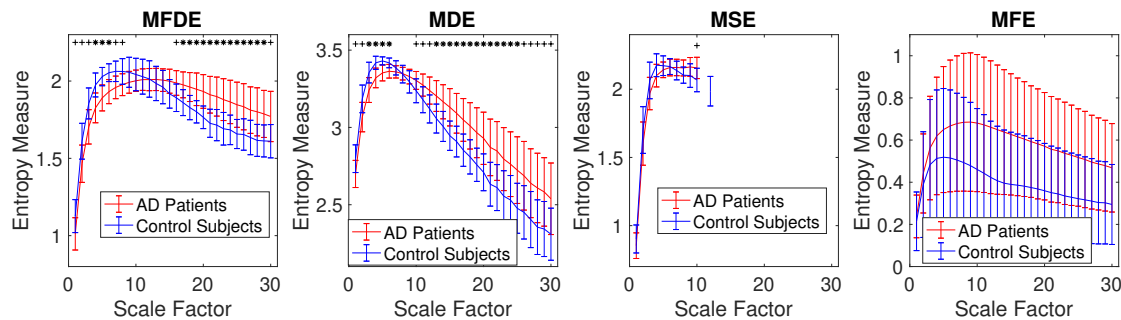
FIGURE 16: Mean value and SD of results of the MFDE, MDE, MSE, and MFE for 11 AD subjects vs. 11 age-matched controls. The scale factors with *p*-values between 0.01 and 0.05, and smaller than 0.01 are respectively shown with + and *. The MSE values are undefined at high scale factors.

recorded from the ataxia patients. This is consistent with the fact that oculomotor impairment is dramatic and a core clinical feature of cerebellar ataxia, whereas eye movement abnormalities in Parkinson's disease are relatively mild.

The Mann-Whitney *U*-test *p*-values show that only MFDE was significantly different in parkinsonism and ataxia patients across the range of scale factors. This shows that where the mean value of a time series noticeably changes along the signal, MFDE may be better than MFE, MSE, and MDE in detecting different states of physiological data.

On the whole, the results support that, in general, MDE and MFDE perform better than MSE and MFE based on Mann-Whitney *U*-test *p*-values and CV values. MSE values were undefined for high scale factors. We also showed that MSE and MFE are considerably slower than MDE and MFDE in Table 5. Thus, we recommend MFDE and MDE over MSE and MFE for the analysis of physiological recordings. Between MDE and MFDE, based on the *p*-values, MDE was better than MFDE only for the dataset of walking stride interval signals for young, elderly, and PD subjects (Fig. 14). However, MFDE outperformed MDE for the characterization of three neurological datasets: 1) focal vs. non-focal EEGs (Fig. 13); 2) stride interval fluctuations for Huntington's disease vs. amyotrophic lateral sclerosis (Fig. 15); and 3) eye movement data for parkinsonism vs. ataxia (Fig. 17). In addition, MFDE results for pink noise were more stable than those for MDE (Fig. 8). Furthermore, MFDE was slightly faster than MDE (Table 5). In sum, the results indicate that MFDE was the fastest and most consistent technique to distinguish various dynamics of the synthetic and real data, especially when dealing with the presence of baseline wanders, or trends, in signals.

V. FUTURE WORK

In spite of the promising findings based on MFDE and MDE, these novel signal processing approaches should be employed on various physiological datasets with a higher number of subjects in order to evaluate their ability for detection of dynamical variability of different kinds of time series.

The physiological nature of the findings for AD vs. controls needs to be further investigated to understand why AD

patients' EEGs are less complex at low scale factors while the controls' recording are less complex at high temporal scales. With regard to eye movement, the higher complexity signal in PD compared with ataxia can be coarsely explained by the fact that eye movements are more impaired in ataxia. However, in future work we hope to better understand more precisely how and why abnormalities seen in ataxia result in a lower complexity signal.

In this article, the most commonly used coarse-graining process was used [8], [9], [16], [23]. The alternative coarse-graining processes based on empirical mode decomposition and finite impulse response (FIR) filters [24] can be employed instead of the classical implementation of coarse-graining process used herein. The multivariate extension of MFDE dealing with both the time and spatial domain at the same time can also be developed.

VI. CONCLUSIONS

In this paper, we introduced MFDE to quantify the complexity of time series based on their fluctuation-based dispersion patterns. The results on synthetic data showed that MFDE, MDE, MFE, and MSE lead to similar findings although MSE values were undefined at high scales. This fact, together with their lower coefficient of variations and much faster computational time, makes us recommend MFDE and MDE over MSE and MFE for the analysis of biomedical signals. Based on the Mann-Whitney *U*-test *p*-values, MDE outperformed MFDE only for the dataset of walking stride interval signals for young, elderly, and PD subjects. Both the MDE and MFDE methods significantly discriminated the AD patients from healthy controls. However, MFDE was better than MDE for the characterization of three neurological datasets: 1) focal vs. non-focal EEGs; 2) stride interval fluctuations for Huntington's disease vs. amyotrophic lateral sclerosis; and 3) eye movement data for Parkinson's disease vs. ataxia, potentially because MFDE is robust to changes in the mean value of a time series, as seen in the eye movement dataset. Additionally, MFDE, compared with MDE, led to more stable entropy values over the scale factors for pink noise. These observations suggest that MFDE may be better than MSE and MDE in detecting different states of synthetic and physiological recordings. We expect MFDE, in addition to
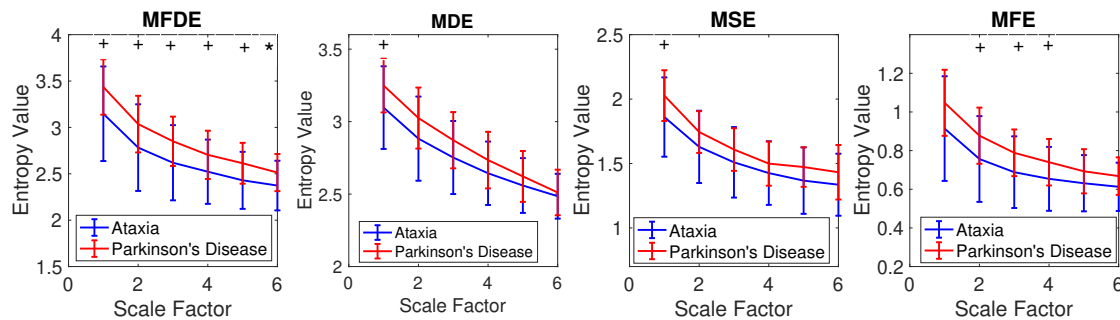
FIGURE 17: Mean value and SD of results obtained by the MFDE, MDE, MSE, and MFE techniques computed from the ataxia' and parkinsonism subjects' eye movement recordings. The scale factors with p-values between 0.01 and 0.05, and smaller than 0.01 are respectively shown with + and *.

MDE, to be widely used for the characterization of different physiologic data in various neurological diseases.

REFERENCES

[1] S. M. Pincus, "Approximate entropy as a measure of system complexity.," *Proceedings of the National Academy of Sciences*, vol. 88, no. 6, pp. 2297–2301, 1991.

[2] J. S. Richman and J. R. Moorman, "Physiological time-series analysis using approximate entropy and sample entropy," *American Journal of Physiology-Heart and Circulatory Physiology*, vol. 278, no. 6, pp. H2039–H2049, 2000.

[3] C. Bandt and B. Pompe, "Permutation entropy: a natural complexity measure for time series," *Physical review letters*, vol. 88, no. 17, p. 174102, 2002.

[4] M. Rostaghi and H. Azami, "Dispersion entropy: A measure for time series analysis," *IEEE Signal Processing Letters*, vol. 23, no. 5, pp. 610–614, 2016.

[5] C. E. Shannon, "A mathematical theory of communication," *ACM SIG-MOBILE Mobile Computing and Communications Review*, vol. 5, no. 1, pp. 3–55, 2001.

[6] S. Sanei and J. A. Chambers, *EEG signal processing*. John Wiley & Sons, 2007.

[7] W. Chen, Z. Wang, H. Xie, and W. Yu, "Characterization of surface emg signal based on fuzzy entropy," *Neural Systems and Rehabilitation Engineering, IEEE Transactions on*, vol. 15, no. 2, pp. 266–272, 2007.

[8] M. Costa, A. L. Goldberger, and C.-K. Peng, "Multiscale entropy analysis of biological signals," *Physical Review E*, vol. 71, no. 2, p. 021906, 2005.

[9] H. Azami, A. Fernández, and J. Escudero, "Refined multiscale fuzzy entropy based on standard deviation for biomedical signal analysis," *Medical & Biological Engineering & Computing*, vol. 55, no. 11, pp. 2037–2052, 2017.

[10] M. Costa, A. L. Goldberger, and C.-K. Peng, "Multiscale entropy analysis of complex physiologic time series," *Physical Review Letters*, vol. 89, no. 6, p. 068102, 2002.

[11] A. Humeau-Heurtier, "The multiscale entropy algorithm and its variants: A review," *Entropy*, vol. 17, no. 5, pp. 3110–3123, 2015.

[12] Y. Bar-Yam, *Dynamics of complex systems*, vol. 213. Addison-Wesley Reading, MA, 1997.

[13] H. C. Fogedby, "On the phase space approach to complexity," *Journal of statistical physics*, vol. 69, no. 1-2, pp. 411–425, 1992.

[14] Y.-C. Zhang, "Complexity and 1/f noise. a phase space approach," *Journal de Physique I*, vol. 1, no. 7, pp. 971–977, 1991.

[15] L. E. V. Silva, B. C. T. Cabella, U. P. da Costa Neves, and L. O. M. Junior, "Multiscale entropy-based methods for heart rate variability complexity analysis," *Physica A: Statistical Mechanics and its Applications*, vol. 422, pp. 143–152, 2015.

[16] F. C. Morabito, D. Labate, F. La Foresta, A. Bramanti, G. Morabito, and I. Palamara, "Multivariate multi-scale permutation entropy for complexity analysis of Alzheimer's disease EEG," *Entropy*, vol. 14, no. 7, pp. 1186–1202, 2012.

[17] S.-D. Wu, C.-W. Wu, S.-G. Lin, K.-Y. Lee, and C.-K. Peng, "Analysis of complex time series using refined composite multiscale entropy," *Physics Letters A*, vol. 378, no. 20, pp. 1369–1374, 2014.

[18] J. Zheng, J. Cheng, Y. Yang, and S. Luo, "A rolling bearing fault diagnosis method based on multi-scale fuzzy entropy and variable predictive model-based class discrimination," *Mechanism and Machine Theory*, vol. 78, pp. 187–200, 2014.

[19] M. Hortelano, R. Reilly, F. Castells, and R. Cervigón, "Refined multiscale fuzzy entropy to analyse post-exercise cardiovascular response in older adults with orthostatic intolerance," *Entropy*, vol. 20, no. 11, p. 860, 2018.

[20] Q. Liu, H. Pan, J. Zheng, J. Tong, and J. Bao, "Composite interpolation-based multiscale fuzzy entropy and its application to fault diagnosis of rolling bearing," *Entropy*, vol. 21, no. 3, p. 292, 2019.

[21] S.-D. Wu, C.-W. Wu, and A. Humeau-Heurtier, "Refined scale-dependent permutation entropy to analyze systems complexity," *Physica A: Statistical Mechanics and its Applications*, vol. 450, pp. 454–461, 2016.

[22] H. Azami and J. Escudero, "Amplitude-and fluctuation-based dispersion entropy," *Entropy*, vol. 20, no. 3, p. 210, 2018.

[23] H. Azami, M. Rostaghi, D. Abásolo, and J. Escudero, "Refined composite multiscale dispersion entropy and its application to biomedical signals," *IEEE Transactions on Biomedical Engineering*, vol. 64, no. 12, pp. 2872–2879, 2017.

[24] H. Azami and J. Escudero, "Coarse-graining approaches in univariate multiscale sample and dispersion entropy," *Entropy*, vol. 20, no. 2, p. 138, 2018.

[25] A. L. Goldberger and M. D. Costa, "Complexity based methods and systems for detecting depression," Aug. 7 2014. US Patent App. 14/233,999.

[26] C.-C. Chung, J.-H. Kang, R.-Y. Yuan, D. Wu, C.-C. Chen, N.-F. Chi, P.-C. Chen, and C.-J. Hu, "Multiscale entropy analysis of electroencephalography during sleep in patients with parkinson disease," *Clinical EEG and neuroscience*, vol. 44, no. 3, pp. 221–226, 2013.

[27] M. M. Rahman, M. I. H. Bhuiyan, and A. R. Hassan, "Sleep stage classification using single-channel eog," *Computers in biology and medicine*, vol. 102, pp. 211–220, 2018.

[28] V. Miskovic, K. J. MacDonald, L. J. Rhodes, and K. A. Cote, "Changes in eeg multiscale entropy and power-law frequency scaling during the human sleep cycle," *Human brain mapping*, vol. 40, no. 2, pp. 538–551, 2019.

[29] H. Azami, E. Kinney-lang, A. Ebied, A. Fernández, and J. Escudero, "Multiscale dispersion entropy for the regional analysis of resting-state magnetoencephalogram complexity in alzheimer's disease," in *Engineering in*

Medicine and Biology Society (EMBC), 2017 39th Annual International Conference of the IEEE, pp. 3182–3185, IEEE, 2017.

[30] K. Hu, P. C. Ivanov, Z. Chen, P. Carpena, and H. E. Stanley, "Effect of trends on detrended fluctuation analysis," Physical Review E, vol. 64, no. 1, p. 011114, 2001.

[31] Z. Wu, N. E. Huang, S. R. Long, and C.-K. Peng, "On the trend, detrending, and variability of nonlinear and nonstationary time series," Proceedings of the National Academy of Sciences, vol. 104, no. 38, pp. 14889–14894, 2007.

[32] C.-K. Peng, S. Havlin, H. E. Stanley, and A. L. Goldberger, "Quantification of scaling exponents and crossover phenomena in nonstationary heartbeat time series," Chaos: An Interdisciplinary Journal of Nonlinear Science, vol. 5, no. 1, pp. 82–87, 1995.

[33] A. Humeau-Heurtier, C.-W. Wu, S. De Wu, M. Guillaume, and P. Abraham, "Refined multiscale hilbert-huang spectral entropy and its application to central and peripheral cardiovascular data," IEEE Transactions on Biomedical Engineering, pp. 1–11, 2016.

[34] H. Azami and J. Escudero, "Improved multiscale permutation entropy for biomedical signal analysis: Interpretation and application to electroencephalogram recordings," Biomedical Signal Processing and Control, vol. 23, pp. 28–41, 2016.

[35] J. Lam, "Preserving useful info while reducing noise of physiological signals by using wavelet analysis," pp. 1–20, 2011.

[36] C. Houdré, D. M. Mason, P. Reynaud-Bouret, and J. Rosinski, High Dimensional Probability VII. Springer, 2016.

[37] D. Labate, F. La Foresta, G. Morabito, I. Palamara, and F. C. Morabito, "Entropic measures of EEG complexity in Alzheimer's disease through a multivariate multiscale approach," Sensors Journal, IEEE, vol. 13, no. 9, pp. 3284–3292, 2013.

[38] A. C. Yang, S.-J. Wang, K.-L. Lai, C.-F. Tsai, C.-H. Yang, J.-P. Hwang, M.-T. Lo, N. E. Huang, C.-K. Peng, and J.-L. Fuh, "Cognitive and neuropsychiatric correlates of EEG dynamic complexity in patients with Alzheimer's disease," Progress in Neuro-Psychopharmacology and Biological Psychiatry, vol. 47, pp. 52–61, 2013.

[39] R. G. Andrzejak, K. Schindler, and C. Rummel, "Nonrandomness, nonlinear dependence, and nonstationarity of electroencephalographic recordings from epilepsy patients," Physical Review E, vol. 86, no. 4, p. 046206, 2012.

[40] J. M. Hausdorff, P. L. Purdon, C. Peng, Z. Ladin, J. Y. Wei, and A. L. Goldberger, "Fractal dynamics of human gait: stability of long-range correlations in stride interval fluctuations," Journal of Applied Physiology, vol. 80, no. 5, pp. 1448–1457, 1996.

[41] U. R. Acharya, Y. Hagiwara, S. N. Deshpande, S. Suren, J. E. W. Koh, S. L. Oh, N. Arunkumar, E. J. Ciaccio, and C. M. Lim, "Characterization of focal eeg signals: a review," Future Generation Computer Systems, 2018.

[42] http://ntsa.upf.edu/

[43] J. M. Hausdorff, A. Lertratanakul, M. E. Cudkowicz, A. L. Peterson, D. Kaliton, and A. L. Goldberger, "Dynamic markers of altered gait rhythm in amyotrophic lateral sclerosis," Journal of applied physiology, vol. 88, no. 6, pp. 2045–2053, 2000.

[44] https://www.physionet.org/physiobank/database/gaitdb

[45] B. Goldfarb and S. Simon, "Gait patterns in patients with amyotrophic lateral sclerosis.," Archives of physical medicine and rehabilitation, vol. 65, no. 2, pp. 61–65, 1984.

[46] https://physionet.org/physiobank/database/gaitndd/

[47] Alzheimer's Association, "2017 Alzheimer's disease facts and figures," Alzheimer's & Dementia, vol. 13, no. 4, pp. 325–373, 2017.

[48] R. S. Wilson, E. Segawa, P. A. Boyle, S. E. Anagnos, L. P. Hizel, and D. A. Bennett, "The natural history of cognitive decline in Alzheimer's disease," Psychology and Aging, vol. 27, no. 4, p. 1008, 2012.

[49] J. Dauwels, F. Vialatte, and A. Cichocki, "Diagnosis of Alzheimer's disease from EEG signals: where are we standing?," Current Alzheimer Research, vol. 7, no. 6, pp. 487–505, 2010.

[50] S. Bhat, U. R. Acharya, N. Dadmehr, and H. Adeli, "Clinical neurophysiological and automated EEG-based diagnosis of the Alzheimer's disease," European Neurology, vol. 74, no. 3-4, pp. 202–210, 2015.

[51] D. Abásolo, R. Hornero, P. Espino, D. Alvarez, and J. Poza, "Entropy analysis of the EEG background activity in Alzheimer's disease patients," Physiological measurement, vol. 27, no. 3, p. 241, 2006.

[52] D. Abásolo, J. Escudero, R. Hornero, C. Gómez, and P. Espino, "Approximate entropy and auto mutual information analysis of the electroencephalogram in Alzheimer's disease patients," Medical & biological engineering & computing, vol. 46, no. 10, pp. 1019–1028, 2008.

[53] J. Escudero, D. Abásolo, R. Hornero, P. Espino, and M. López, "Analysis of electroencephalograms in Alzheimer's disease patients with multiscale entropy," Physiological measurement, vol. 27, no. 11, p. 1091, 2006.

[54] T. N. Tombaugh and N. J. McIntyre, "The mini-mental state examination: a comprehensive review," Journal of the American Geriatrics Society, vol. 40, no. 9, pp. 922–935, 1992.

[55] N. Buttner, D. Geschwind, J. C. Jen, S. Perlman, S. M. Pulst, and R. W. Baloh, "Oculomotor phenotypes in autosomal dominant ataxias," Arch Neurol, vol. 55, pp. 1353–7, Oct 1998.

[56] M. Vidailhet, S. Rivaud, N. Gouider-Khouja, B. Pillon, A. M. Bonnet, B. Gaymard, Y. Agid, and C. Pierrot-Deseilligny, "Eye movements in parkinsonian syndromes," Ann Neurol, vol. 35, pp. 420–6, Apr 1994.

[57] K. G. Rottach, D. E. Riley, A. O. DiScenna, A. Z. Zivotofsky, and R. J. Leigh, "Dynamic properties of horizontal and vertical eye movements in parkinsonian syndromes," Ann Neurol, vol. 39, pp. 368–77, Mar 1996.

[58] https://www.ri.cmu.edu/publications/intraface/

[59] A. Humeau-Heurtier, "Multivariate generalized multiscale entropy analysis," Entropy, vol. 18, no. 11, p. 411, 2016.

[60] F. Kaffashi, R. Foglyano, C. G. Wilson, and K. A. Loparo, "The effect of time delay on approximate & sample entropy calculations," Physica D: Nonlinear Phenomena, vol. 237, no. 23, pp. 3069–3074, 2008.

[61] R. Sharma, R. B. Pachori, and U. R. Acharya, "Application of entropy measures on intrinsic mode functions for the automated identification of focal electroencephalogram signals," Entropy, vol. 17, no. 2, pp. 669–691, 2015.

[62] S. Nemati, B. A. Edwards, J. Lee, B. Pittman-Polletta, J. P. Butler, and A. Malhotra, "Respiration and heart rate complexity: effects of age and gender assessed by band-limited transfer entropy," Respiratory physiology & neurobiology, vol. 189, no. 1, pp. 27–33, 2013.

[63] M. U. Ahmed and D. P. Mandic, "Multivariate multiscale entropy: A tool for complexity analysis of multichannel data," Physical Review E, vol. 84, no. 6, p. 061918, 2011.

[64] J. Escudero, E. Acar, A. Fernández, and R. Bro, "Multiscale entropy analysis of resting-state magnetoencephalogram with tensor factorisations in Alzheimer's disease," Brain research bulletin, vol. 119, pp. 136–144, 2015.

[65] H. Azami, D. Abásolo, S. Simons, and J. Escudero, "Univariate and multivariate generalized multiscale entropy to characterise EEG signals in Alzheimer's disease," Entropy, vol. 19, no. 1, p. 31, 2017.

HAMED AZAMI received his PhD in Biomedical Signal Processing from the Institute for Digital Communication, University of Edinburgh, UK, in 2018. He is currently a Postdoctoral Research Fellow in Biomedical Signal Processing and Machine Learning at Massachusetts General Hospital and Harvard University, USA. His main research interests include biomedical signal processing, nonlinear analysis, and machine learning.

Dr. Azami received the prestigious Nightingale Award for the best paper published in 2017 in Medical and Biological Engineering and Computing. He has served as the Guest Editor of the Journal of Complexity as well as the Technical Program Committee Member of the IEEE Machine Learning for Signal Processing and IEEE Conference on Digital Signal Processing.

STEVEN E. ARNOLD received his M.D. from Boston University, USA. Dr. Arnold completed residency training in Psychiatry at the New York State Psychiatric Institute/Columbia Presbyterian Medical Center in New York, and residency training in Neurology at the University of Iowa Hospitals and Clinics in Iowa City. He also completed fellowship training in Behavioral Neurology / Cognitive Neuroscience and was a post-doctoral associate in Neuroanatomy in Iowa. Dr. Arnold is board certified in both neurology and psychiatry. After his training, Dr. Arnold joined the faculty at the University of Pennsylvania where he was Professor of Psychiatry and Neurology until his move to MGH in 2015.

At MGH, Dr. Arnold is leading the Interdisciplinary Brain Center, a new collaboration of the Departments of Neurology, Psychiatry and the Martinos Center for Neuroimaging. Its mission is to facilitate the discovery, development, and implementation of promising therapeutics and associated diagnostics for individuals with complex brain disorders that affect cognition, behavior and emotion. Alzheimer's disease and related disorders are major disease interests of the Interdisciplinary Brain Center.

GUILLERMO SAPIRO was born in Montevideo, Uruguay, on April 3, 1966. He received his B.Sc. (summa cum laude), M.Sc., and Ph.D. from the Department of Electrical Engineering at the Technion, Israel Institute of Technology, in 1989, 1991, and 1993 respectively. After post-doctoral research at MIT, Dr. Sapiro became Member of Technical Staff at the research facilities of HP Labs in Palo Alto, California. He was with the Department of Electrical and Computer Engineering at the University of Minnesota, where he held the position of Distinguished McKnight University Professor and Vincentine Hermes-Luh Chair in Electrical and Computer Engineering. Currently he is the Edmund T. Pratt, Jr. School Professor with Duke University.

G. Sapiro works on theory and applications in computer vision, computer graphics, medical imaging, image analysis, and machine learning. He has authored and co-authored over 400 papers in these areas and has written a book published by Cambridge University Press, January 2001. G. Sapiro was awarded the Gutwirth Scholarship for Special Excellence in Graduate Studies in 1991, the Ollendorff Fellowship for Excellence in Vision and Image Understanding Work in 1992, the Rothschild Fellowship for Post-Doctoral Studies in 1993, the Office of Naval Research Young Investigator Award in 1998, the Presidential Early Career Awards for Scientist and Engineers (PECASE) in 1998, the National Science Foundation Career Award in 1999, and the National Security Science and Engineering Faculty Fellowship in 2010. He received the test of time award at ICCV 2011. G. Sapiro is a Fellow of IEEE and SIAM. G. Sapiro was the founding Editor-in-Chief of the SIAM Journal on Imaging Sciences.

SAEID SANEI (SM'05) received his PhD in signal processing from Imperial College London, UK. His research interests include adaptive and nonlinear signal processing, cooperative learning, multi-way and multimodal signal processing, and compressive sensing. He has served as an Associate Editor for the IEEE Signal Processing Letters, IEEE Signal Processing Magazine, and Journal of Computational Intelligence and Neuroscience. He has published four monograms, a number of book chapters, and over 360 papers in peer reviewed journals and conference proceedings. He has served as the TCM for the IEEE MLSP and SPTM committees. He is currently a Professor of Signal Processing and Machine Learning in the UK.

JAVIER ESCUDERO (S'07, M'10) received the MEng and PhD degrees in telecommunications engineering from the University of Valladolid, Spain, in 2005 and 2010, respectively. Afterwards, he held a post-doctoral position at Plymouth University, UK, until 2013.

He is currently a tenured academic at the School of Engineering of the University of Edinburgh, UK, where he leads a research group in biomedical signal processing with interests in non-linear analysis, network theory, and multiway decompositions. He is the author of over 55 scientific journal articles.

Dr. Escudero received the Third Prize of the EMBS Student Paper Competition in 2007 and the award to the best PhD thesis in healthcare technologies by the Spanish Organization of Telecommunications Engineers in 2010. In 2016, he was elected member of the Young Academy of Scotland. He has also received the Nightingale Award for the best paper published in 2017 in Medical and Biological Engineering and Computing. He has served as president of the Society of Spanish Researchers in the United Kingdom (SRUK) and of the Network of Spanish Researchers Abroad (RAICEX) during the 2018/19 term.
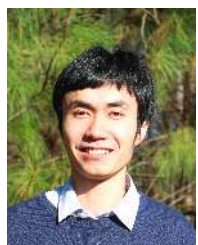
ZHUOQING CHANG Zhuoqing Chang received his BEng in Measuring and Controlling Technologies and Instruments at Tianjin University, China in 2013 and his MSc in Electrical and Computer Engineering at Duke University, USA, in 2014. He is currently working towards the PhD degree in electrical and computer engineering at Duke University. His current research interests include applied computer vision, machine learning, and behavioral coding analysis.

ANOOPUM GUPTA received his undergraduate degree in Electrical Engineering from Georgia Tech, his medical degree from the University of Pittsburgh School of Medicine, and his PhD in Robotics from Carnegie Mellon University's School of Computer Science. He completed his residency in neurology at the Partners-Harvard Neurology Residency Program (MGH and Brigham and Women's Hospital). His clinical interests are in neurogenetic and neurodegenerative diseases in adults and children, in particular those affecting the cerebellum. His research program involves the use of accessible technologies combined with signal processing, computer vision, and machine learning methods to deeply understand the consequences of neurologic disease on motor and cognitive behavior. Broadly he is involved in projects at the intersection of computational science and medicine.

○ ○ ○